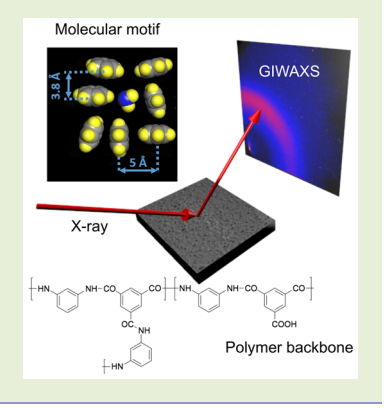
Molecular Structure of Aromatic Reverse Osmosis Polyamide Barrier Lavers

Qinyi Fu,[†]
[®] Nisha Verma,[†] Hongyang Ma,^{†,‡} Francisco J. Medellin-Rodriguez,^{†,§} Ruipeng Li,^{||} Masafumi Fukuto,^{||} Christopher M. Stafford,^{†,®} Benjamin S. Hsiao,^{*,†,®} and Benjamin M. Ocko^{*,||}

Supporting Information

Downloaded via STONY BROOK UNIV SUNY on May 14, 2019 at 02:50:18 (UTC). See https://pubs.acs.org/sharingguidelines for options on how to legitimately share published articles.

ABSTRACT: The molecular structures of polyamide barrier layers in reverse osmosis membranes, made by interfacial polymerization of m-phenylenediamine and trimesoyl chloride under different reaction and post-treatment conditions, were characterized by grazing incidence wide-angle X-ray scattering (GIWAXS). The molecular backbone packing is consistent with two different aromatic molecular packing motifs (parallel and perpendicular) with preferential surface-induced orientation. The results suggest that the perpendicular, T-shaped, packing motif (5 Å spacing) might be associated with optimal membrane permeance, compared with the parallel packings (3.5-4.0 Å spacings).



ost of the earth's water is in the oceans and only 3% is fresh water. Reverse osmosis (RO) has become the leading method of converting seawater into potable water. 1-3 Although RO systems are getting close to their thermodynamic limit, 1,4 thinner and more permeable polyamide barrier layers, with an optimal degree of cross-linking and wettability, have the potential to improve the functional properties, increase permeance, and reduce the costs of water purification. Despite the technical importance of the barrier layer (the smallest pore size component in a RO membrane), an understanding of the relationship between molecular level structure and function has yet to emerge.

The typical polyamide (PA) barrier layer is made by interfacial polymerization (IP) using m-phenylenediamine (MPD) dissolved in water and trimesoyl chloride (TMC) dissolved in hexane. 1,5 In commercial RO membranes, a rapid polymerization reaction occurs when the MPD infiltrated surface of the porous polysulfone substrate is exposed to TMC.^{1,2} This process yields a chemically heterogeneous and rough barrier layer, whose complex morphology and porosity depends on the monomer concentrations and reaction conditions.⁶ The barrier layer morphology has been investigated by TEM, AFM, SEM, 9,10 and SAXS, 11,12 however, these methods have not enabled the determination of the molecular scale structure. MD simulations have provided

insight into the structure formation, 6,13-15 yet full atomistic simulations have only recently emerged.¹⁵

The membrane scientific community has recently focused attention on well-defined model membrane systems since the precise composition and manufacturing conditions of commercial membranes are proprietary and, hence, not reported. In this regard, molecular layer-by-layer PA films have been prepared by Stafford et al. 16 through the sequential and alternating deposition of MPD and TMC solutions on a flat surface to produce smooth, well-controlled barrier layers. Likewise, Karan et al. have reported the formation of polyamide layers via controlled IP reaction on a sacrificial support layer. While subsequent neutron and X-ray reflectivity measurements have shown that the layer thickness is 8-24 nm, 17 the molecular structure of these thin layers has not been ascertained

Surface layering and preferential alignment has been found in thin films of alkyl-side chain polymers, 18 conjugated polymeric thin films 19-21 and vapor deposited glass films, 22 yet it is not known whether these same effects occur in

Received: October 26, 2018 Accepted: February 27, 2019 Published: March 14, 2019

Department of Chemistry, Stony Brook University, Stony Brook, New York 11794, United States

^{*}State Key Laboratory of Organic Inorganic Composites, Beijing University of Chemical Technology, Beijing 100029, People's Republic of China

[§]Universidad Autónoma de San Luis Potosí, FCQ, San Luis Potosí 78210, SLP, México

National Synchrotron Light Source II, Brookhaven National Laboratory, Upton, New York 11973, United States!

¹Materials Science and Engineering Division, National Institute of Standards and Technology, Gaithersburg, Maryland 20899, United States

ACS Macro Letters

Letter

commercial membranes. This is particularly relevant to the barrier layer on RO membranes since such molecular ordering may influence the membrane permeance. Despite the recent progress in making well-defined MPD-TMC PA films, the molecular-scale structure and alignment features of these films has not been reported. We note that there are two bulk studies, 11,23 both limited in scope, whereas no structural model has been presented to describe the results.

In this Letter, we present synchrotron GIWAXS results from well-defined thin PA layers supported on silicon wafers. From the scattering patterns, we show that the polymeric molecular order exhibits several characteristic length scales. A schematic of the film preparation (PA barrier layer) procedure is shown in Figure 1 where additional details are provided in the Experimental Section and the Supporting Information.

2D GIWAXS scattering patterns are shown in Figure 2A,B for 18 nm thick PA films before and after citric acid post-

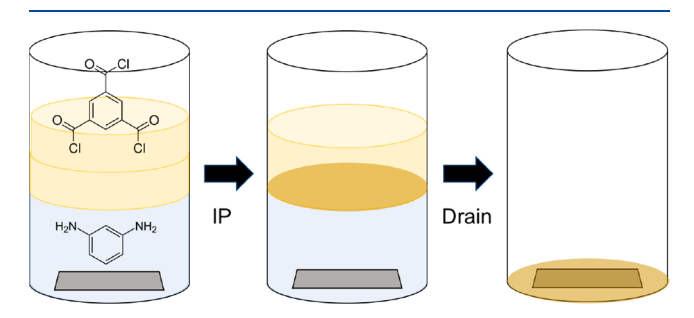


Figure 1. Thin PA films were prepared at the water/hexane interface using MPD and TMC solutions with the assistance of a thin, intermediate buffer layer of hexane between the two solutions (left), and then they were transferred to a polished silicon wafer (right).

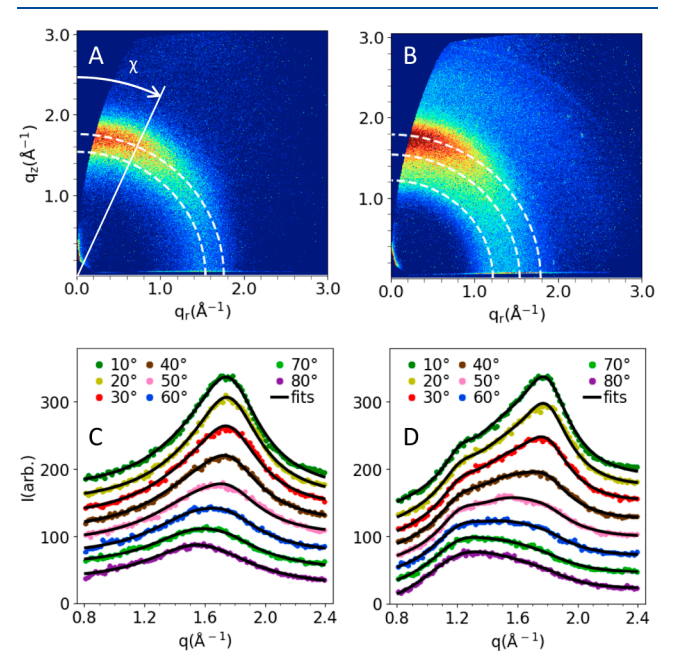


Figure 2. GIWAXS scattering patterns, after the Ewald correction, in reciprocal space from the MPD-TMC PA film in vacuum before (A) and after citric acid post-treatment (B). Dashed arcs (shown for reference) in (A) at 1.54 and 1.76 Å $^{-1}$ and in (B) at 1.22, 1.54, and 1.79 Å $^{-1}$ (C, D). Scattering profiles obtained from (A) and (B) by integrating the intensity over $\pm 2^{\circ}$ in χ . Fits (solid lines) are described in the text.

treatment (see Supporting Information for information on the thickness measurements). In this figure, q_r and q_z correspond to the surface parallel and normal scattering wave vectors, respectively, where the patterns provide information on the molecular structure and preferential orientations. We note that random molecular orientation would give rise to uniform scattering rings, that is, equal intensity at all azimuthal angles (χ) , and this is not observed in our films. Rather, we observe arc-like scattering features, as in Figure 2A,B, where the more intense scattering is preferentially aligned along the surface normal direction, with weaker scattering along the surface parallel direction. Prior to post-treatment (Figure 2A), their arc-like scattering features are centered at and whose broad width is suggestive of an amorphous phase with a short-range order. Closer examination of the image shows that the arc-like scattering features do not lie on a circle (dashed rings as a reference), where quantitative analysis is presented in the Supporting Information. After citric acid treatment, the scattering pattern is radially more diffuse but remains anisotropic. While the reported measurements were on dry films, our measurements carried out with controlled humidity showed similar results (not shown), albeit with higher

To explore the anisotropic nature of the scattering patterns, we plot the scattered intensity versus $q=\sqrt{q_{\rm r}^2+q_{\rm z}^2}$ for different values of χ , where the results are shown in Figures 2C,D. For the untreated sample (Figure 2C), the peak intensity decreases and moves to smaller q as χ is increased. At $\chi=10^\circ$ and 80° , the peaks are centered at 1.75 and 1.55 Å⁻¹, respectively.

To quantify the scattering data (position, width, and intensity), we fit the scattering profiles with Lorentzian functions.²⁴ For $\chi = 80^{\circ}$, the profile is well described by a single Lorentzian scattering profile (black line) and a sloping background, $I_1 \times (1 + (q - q_1)^2 \Delta_1^{-2})^{-1} + a + bq$, with $q_1 = 1.54$ Å⁻¹ and width $\Delta_1 = 0.40$ Å⁻¹ (note that the peak's profile falls off too slowly with q for a Gaussian profile to describe the shape). The correlation length of this analysis, $\xi_1 = 0.93 \ \pi/\Delta_1$ \cong 7 Å (based on the Debye-Scherer formula), is short and indicates an amorphous structure, where the scattering profile shape is sensitive to the correlations between only several neighboring backbone segments. The profiles for the smallest χ angles (Figure 2A) are asymmetric and cannot be represented by a single Lorentzian with a symmetric profile shape. However, all χ profiles are reasonably well described by fits that are composed by the sum of two Lorentzian scattering profiles (Supporting Information) with the same constant peak positions of $q_1 = 1.54$ Å⁻¹ and $q_2 = 1.76$ Å⁻¹ and respective widths $\Delta_1 = 0.40$ Å⁻¹ and $\Delta_2 = 0.25$ Å⁻¹ (q_1 and Δ_1 are those obtained for the $\chi = 80^{\circ}$ fit), where q_1 and q_2 correspond to molecular spacings, $2\pi/q$ of 4.0 and 3.5 Å, respectively. These q_2 and Δ_2 values (Δ_2 corresponds to a 12 Å correlation length) give the best overall fits, where for each profile there are two independent intensities and two background terms. The linear background term can be attributed in part to multiple, broad higher order scattering features that do not give rise to identifiable peaks. The existence of two independent, scattering peaks suggests that there are two characteristic local molecular spacings, where the corresponding distribution between the two peaks provides a measure of their orientation dependence (Supporting Information).

ACS Macro Letters Letter

In the GIWAXS profiles, before and after the citric acid treatment (Figure 2C,D), the films exhibit slightly different scattering features. There is significantly more scattering at lower q values in the treated film (Figure 2D), suggesting a structure of domains with a larger characteristic molecular spacing. This is particularly apparent for the larger χ values (e.g., 80°) that exhibit an extremely broad scattering feature centered at $\sim 1.3 \text{ Å}^{-1}$, whereas a well-defined peak remains at ~1.75 Å⁻¹ for the small χ values (e.g., 10°), as observed in the untreated film. With increasing χ values, the scattering features move to lower q values and appear much broader compared to the untreated sample. To describe the treated scattering profiles, a third Lorentzian term is required. In the first fitting cycle, we let parameters for all three Lorentzian profiles vary at each χ . After determining that many parameters did not depend significantly with χ , we fixed $q_1 = 1.54 \text{ Å}^{-1}$, $q_2 = 1.79$ ${\rm \AA}^{-1}$, $q_3 = 1.22 {\rm \AA}^{-1}$, $\Delta_1 = 0.40 {\rm \AA}^{-1}$ and $\Delta_2 = 0.18 {\rm \AA}^{-1}$ in subsequent fits. The q_3 peak corresponds to a ~ 5 Å spacing, a larger distance than those corresponding to the untreated film. At each χ , three peak intensities, background parameters, and Δ_3 were varied in the final fitting. With increasing χ , Δ_3 increases monotonically from 0.11 to 0.30 Å⁻¹, corresponding to a maximum correlation length of 26 Å at $\chi = 10^{\circ}$, a factor of 3-4 larger than for the other peaks.

The scattering features with a 5 Å spacing are not randomly distributed, rather, they are preferentially aligned along the surface parallel direction where the scattering peaks centered at q_1 and q_2 are the weakest (Supporting Information). In the fitting, note that q_1 and Δ_1 are the same as the untreated values and q_2 and Δ_2 are only slightly different from their untreated values. Further discussion of the fitting and fitted parameters can be found in the Supporting Information.

We conjecture that the scattering in the $1-2 \text{ Å}^{-1}$ range is dominated by the packing of the aromatic ring moieties, since most of the atoms are in the aromatic rings and fewer are in the linker regions between chains (amide bonds). The broad peaks at q_1 and q_2 correspond to molecular spacings of 4.0 and 3.5 Å, respectively, are consistent with parallel, " $\pi - \pi$ " stacking of the aromatic cores²⁵ and not from the intrinsic spacing of water channels. Well-controlled MPD-TMC PA films, made using a layer-by-layer process, show a symmetric, single broad peak that is well described by a Lorentzian fit with $q = 1.71 \text{ Å}^{-1}$ and $\Delta = 0.40~\mbox{Å}^{-1,26}$ similar to the untreated film shown in Figure 2C. Furthermore, we have determined that bulk MPD-TMC PA powders made by gradual mixing of MPD and TMC solutions can be described by a uniformly oriented, single peak $q = 1.70 \text{ Å}^{-1}$ and $\Delta = 0.27 \text{ Å}^{-1}$ (Supporting Information), similar to our untreated film. These results suggest that slow preparation procedures give rise to molecular spacings, consistent with parallel " $\pi - \pi$ " stacking, whereas faster reaction processes and post-treatments give rise to other features. In aromatic molecular systems, the parallel stacking may be either parallel face-centered or parallel offset, 25 but in polymer systems, steric constraints can give rise to a greater distribution in the packing motifs. For instance, the 3.8 Å " π – π spacing" in P3HT is reasonably consistent with our findings. 19 For the untreated bulk and the layer-by-layer samples, there is no indication of a 5 Å spacing, such as the one observed for films after the acid treatment.

The 5 Å spacing $(q = 1.22 \text{ Å}^{-1})$ observed after citric acid treatment is consistent with the perpendicular packing of neighboring aromatic cores in the so-called "T-shaped" configuration. ^{15,25,27} The larger spacing appears to be better

associated with effective filtration materials (discussed below) than those with 3.5–4.0 Å spacings. The scattering peak at 1.22 Å $^{-1}$ exhibits considerable variation with the orientation of q, both in intensity and width, and supports our hypothesis that the in-plane and out-of-plane structures are not the same, suggestive of an interface-induced process. A previous wide-angle X-ray scattering study of the structure of MPD-TMC PA materials 11,12 reported a single, broad peak between 1.16 to 1.22 Å $^{-1}$ (5.1–5.4 Å), in general agreement with our findings.

GIWAXS studies (Supporting Information) of a commercial BWXLE (DOW Filmtec) RO membrane provides additional insight into the molecular structure of PA barrier layers. In part, this membrane was selected since it does not have a bound terminal hydrophilic layer. Here the PA/PS film is soaked in distilled water for an hour and subsequently dried, then placed with the PA surface in smooth contact with the silicon wafer where the PS film is subsequently removed, and rinsed using organic solvents.²⁸ The GIWAXS pattern from the BWXLE membranes exhibit similar arc-like scattering features with characteristic peak positions (very similar to the pattern shown in Figure 2B). The structural similarities appear to validate that our well-defined membranes share some common structural motifs as commercial membranes. A full comparison is complicated since the GIWAXS patterns for commercial MPD-TMC PA membranes depend on the commercial product, the solvent used to remove the polysulfone layer, and whether the membrane was first exposed to water compaction. Due to this variability and since this is not the primary subject of this Letter, a separate publication will further explore these details.²⁹

The water diffusion through a heterogeneous, randomly cross-linked PA matrix is influenced both by the nanoscale channels formed during the cross-linking process and by the assembly of local molecular structural motifs. The latter is determined by the interactions between the aromatic rings, which are constrained by steric interactions due to the molecular connectivity along the polymer backbone. Based on the results from well-formed films and both bulk and commercial materials, we speculate that the T-shaped, perpendicular aromatic packing motif of the aromatic cores may provide preferred conditions for water diffusion since its structure is presumably lower in density and not as compact as the parallel stacking arrangement (Figure 3). Although the Tshaped configuration has been reported in MD simulations¹⁵ of PA materials, its role on water transport has not been considered before.

Our studies clearly show that the short-range molecular scale structure in an 18 nm thick, MPD-TMC PA film can be explored in great detail using synchrotron GIWAXS methods. The resulting film structure exhibits anisotropy related to the film growth direction where the molecular basis of the anisotropy remains an open question. Our results from chemically treated films and a commercial membrane suggest that the 5 Å spacing associated with the T-shaped configuration may play an important role in governing the membrane permeance. Future GIWAXS studies on a variety of films made under different conditions, monomers and post-treatments, along with careful depth dependence measurements obtained by varying the incident angle, have the potential to provide a detailed structure—function relationship for polyamide barrier layers.

ACS Macro Letters

Letter

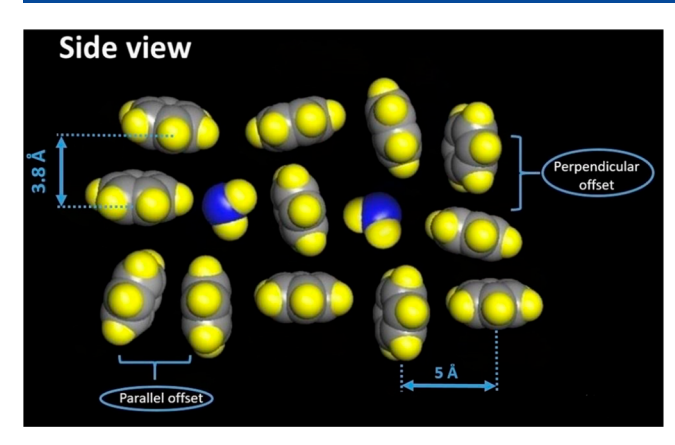


Figure 3. Schematic of aromatic molecular packing motifs in a PA matrix (the connecting atoms between the aromatic rings are not shown), containing parallel and perpendicular arrangement along with water molecules.

EXPERIMENTAL SECTION

The film preparation procedure is shown in Figure 1. The MPD—water solution (0.1 wt %) is added to a clean beaker with a silicon wafer on the bottom, the hexane buffer layer is added on top, followed by the dropwise addition of the TMC—hexane solution (0.04 wt %), and the PA film is deposited on the silicon by draining the solution. The buffer layer prevents immediate mixing and polymerization that is thought to lead to the observed chemical heterogeneity and surface roughness in commercial membranes. To remove unreacted MPD monomers, a post-treatment using 1 wt % citric acid was carried out. In the absence of this post-treatment and depending on the yield of the polymerization reaction, the GIWAXS patterns sometimes exhibit sharp crystalline peaks associated with unreacted MPD monomers. The acid treatment also serves to protonate unreacted carboxylic acid groups which could disrupt internal hydrogen bonding and ultimately lead to structural changes within the membrane.

ASSOCIATED CONTENT

S Supporting Information

The Supporting Information is available free of charge on the ACS Publications website at DOI: 10.1021/acsmacrolett.9b00077.

Experimental details and supporting figures (PDF).

AUTHOR INFORMATION

Corresponding Authors

*E-mail: ocko@bnl.gov.

*E-mail: benjamin.hsiao@stonybrook.edu.

ORCID ®

Qinyi Fu: 0000-0003-3818-3757

Christopher M. Stafford: 0000-0002-9362-8707 Benjamin S. Hsiao: 0000-0002-3180-1826 Benjamin M. Ocko: 0000-0003-2596-1206

Notes

The authors declare no competing financial interest.

ACKNOWLEDGMENTS

The Stony Brook team thanks the financial support from the Polymers Program, Division of Materials Research of the National Science Foundation (DMR-1808690). Work carried out at the Complex Materials Scattering (CMS/11- BM) and Soft Matter Interfaces (SMI/12ID) beamlines at the National Synchrotron Light Source II, and the Center for Functional

Nanomaterials, is supported by the U.S. DOE Office of Science Facilities, at Brookhaven National Laboratory under Contract DE- SC0012704. We thank Mikhail Zhernenkov, Hans-Georg Steinrück, Yugang Zhang, and Dmytro Nykypanchuk for discussions and their assistance.

DEDICATION

Dedicated to Prof. Peter Pershan (Harvard University), a pioneer of the field of x-ray scattering studies of liquid surfaces and thin organic films, on his 85th birthday.

REFERENCES

- (1) Elimelech, M.; Phillip, W. A. The future of seawater desalination: energy, technology, and the environment. *Science* **2011**, 333 (6043), 712–7.
- (2) Karan, S.; Jiang, Z.; Livingston, A. G. Sub-10 nm polyamide nanofilms with ultrafast solvent transport for molecular separation. *Science* **2015**, 348 (6241), 1347–51.
- (3) Darling, S. B. Perspective: Interfacial materials at the interface of energy and water. *J. Appl. Phys.* **2018**, *124* (3), 030901.
- (4) Shrivastava, A.; Rosenberg, S.; Peery, M. Energy efficiency breakdown of reverse osmosis and its implications on future innovation roadmap for desalination. *Desalination* **2015**, 368, 181–192.
- (5) Giwa, A.; Akther, N.; Dufour, V.; Hasan, S. W. A critical review on recent polymeric and nano-enhanced membranes for reverse osmosis. *RSC Adv.* **2016**, *6* (10), 8134–8163.
- (6) Oizerovich-Honig, R.; Raim, V.; Srebnik, S. Simulation of thin film membranes formed by interfacial polymerization. *Langmuir* **2010**, 26 (1), 299–306.
- (7) Freger, V.; Gilron, J.; Belfer, S. TFC polyamide membranes modified by grafting of hydrophilic polymers: an FT-IR/AFM/TEM study. *J. Membr. Sci.* **2002**, 209 (1), 283–292.
- (8) Kwak, S. Y.; Jung, S. G.; Yoon, Y. S.; Ihm, D. W. Details of surface features in aromatic polyamide reverse osmosis membranes characterized by scanning electron and atomic force microscopy. *J. Polym. Sci., Part B: Polym. Phys.* **1999**, 37 (13), 1429–1440.
- (9) Chong, C. Y.; Lau, W. J.; Yusof, N.; Lai, G. S.; Othman, N. H.; Matsuura, T.; Ismail, A. F. Studies on the properties of RO membranes for salt and boron removal: Influence of thermal treatment methods and rinsing treatments. *Desalination* **2018**, 428, 218–226.
- (10) Elimelech, M.; Zhu, X. H.; Childress, A. E.; Hong, S. K. Role of membrane surface morphology in colloidal fouling of cellulose acetate and composite aromatic polyamide reverse osmosis membranes. *J. Membr. Sci.* **1997**, *127* (1), 101–109.
- (11) Singh, P. S.; Ray, P.; Xie, Z.; Hoang, M. Synchrotron SAXS to probe cross-linked network of polyamide 'reverse osmosis' and 'nanofiltration' membranes. *J. Membr. Sci.* **2012**, *421*, 51–59.
- (12) Culp, T. E.; Ye, D.; Paul, M.; Roy, A.; Behr, M. J.; Jons, S.; Rosenberg, S.; Wang, C.; Gomez, E. W.; Kumar, M.; Gomez, E. D. Probing the Internal Microstructure of Polyamide Thin-Film Composite Membranes Using Resonant Soft X-ray Scattering. ACS Macro Lett. 2018, 7 (8), 927–932.
- (13) Muscatello, J.; Muller, E. A.; Mostofi, A. A.; Sutton, A. P. Multiscale molecular simulations of the formation and structure of polyamide membranes created by interfacial polymerization. *J. Membr. Sci.* **2017**, *527*, 180–190.
- (14) Harder, E.; Walters, D. E.; Bodnar, Y. D.; Faibish, R. S.; Roux, B. Molecular dynamics study of a polymeric reverse osmosis membrane. *J. Phys. Chem. B* **2009**, *113* (30), 10177–82.
- (15) Wei, T.; Zhang, L.; Zhao, H.; Ma, H.; Sajib, M. S.; Jiang, H.; Murad, S. Aromatic Polyamide Reverse-Osmosis Membrane: An Atomistic Molecular Dynamics Simulation. *J. Phys. Chem. B* **2016**, *120* (39), 10311–10318.
- (16) Gu, J. E.; Lee, S.; Stafford, C. M.; Lee, J. S.; Choi, W.; Kim, B. Y.; Baek, K. Y.; Chan, E. P.; Chung, J. Y.; Bang, J.; Lee, J. H.

ACS Macro Letters

Molecular layer-by-layer assembled thin-film composite membranes for water desalination. *Adv. Mater.* **2013**, *25* (34), 4778–82.

- (17) Foglia, F.; Karan, S.; Nania, M.; Jiang, Z. W.; Porter, A. E.; Barker, R.; Livingston, A. G.; Cabral, J. T. Neutron Reflectivity and Performance of Polyamide Nanofilms for Water Desalination. *Adv. Funct. Mater.* **2017**, 27 (37), 1701738.
- (18) Prasad, S.; Jiang, Z.; Sinha, S. K.; Dhinojwala, A. Partial crystallinity in alkyl side chain polymers dictates surface freezing. *Phys. Rev. Lett.* **2008**, *101* (6), 065505.
- (19) Kline, R. J.; Mcgehee, M. D.; Toney, M. F. Highly oriented crystals at the buried interface in polythiophene thin-film transistors. *Nat. Mater.* **2006**, *5* (3), 222–228.
- (20) Hlaing, H.; Lu, X.; Hofmann, T.; Yager, K. G.; Black, C. T.; Ocko, B. M. Nanoimprint-induced molecular orientation in semi-conducting polymer nanostructures. *ACS Nano* **2011**, *5* (9), 7532–8.
- (21) Aryal, M.; Trivedi, K.; Hu, W. W. Nano-confinement induced chain alignment in ordered P3HT nanostructures defined by nanoimprint lithography. ACS Nano 2009, 3 (10), 3085–90.
- (22) Gujral, A.; O'Hara, K. A.; Toney, M. F.; Chabinyc, M. L.; Ediger, M. D. Structural Characterization of Vapor-Deposited Glasses of an Organic Hole Transport Material with X-ray Scattering. *Chem. Mater.* **2015**, 27 (9), 3341–3348.
- (23) Matthews, T. Growth Dynamics, Charge Density, And Structure of Polyamide Thin-Film Composite Membranes; University of Illinois at Urbana-Champaign, 2014.
- (24) Factor, B. J.; Russell, T. P.; Toney, M. F. Grazing-Incidence X-Ray-Scattering Studies of Thin-Films of an Aromatic Polyimide. *Macromolecules* **1993**, 26 (11), 2847–2859.
- (25) Martinez, C. R.; Iverson, B. L. Rethinking the term "pi-stacking. *Chemical Science* **2012**, 3 (7), 2191–2201.
- (26) Stafford, C. M.; Fu, Q.; Hsiao, B. S.; Ocko, B. M., Unpublished work
- (27) Sinnokrot, M. O.; Sherrill, C. D. Substituent effects in pi-pi interactions: sandwich and T-shaped configurations. *J. Am. Chem. Soc.* **2004**, *126* (24), *7690–7*.
- (28) Freger, V. Swelling and morphology of the skin layer of polyamide composite membranes: an atomic force microscopy study. *Environ. Sci. Technol.* **2004**, *38* (11), 3168–75.
- (29) Fu, Q.; Verma, N.; Stafford, C. M.; Hsiao, B. S.; Ocko, B. M., Unpublished work.